www.sciencemag.org/content/363/6433/1345/suppl/DC1

Supplementary Materials for

High-fructose corn syrup enhances intestinal tumor growth in mice

Marcus D. Goncalves, Changyuan Lu, Jordan Tutnauer, Travis E. Hartman, Seo-Kyoung Hwang, Charles J Murphy, Chantal Pauli, Roxanne Morris, Sam Taylor, Kaitlyn Bosch, Sukjin Yang, Yumei Wang, Justin Van Riper, H Carl Lekaye, Jatin Roper, Young Kim, Qiuying Chen, Steven S. Gross, Kyu Y. Rhee, Lewis C. Cantley*, Jihye Yun*

*Corresponding author. Email: jihye.yun@bcm.edu (J.Y.); lcantley@med.cornell.edu (L.C.C.)

Published 22 March 2019, *Science* **363**, 1345 (2019)
DOI: 10.1126/science.aat8515

This PDF file includes:

Materials and Methods

Animal study

A genetically engineered mouse model of intestinal tumorigenesis, *Lgr5-EGFP-IRES-creERT2; Apc$^{flox/flox}$* (referred as APC$^{-/-}$) mice, in C57BL/6 background were generated as described previously (*11*). Compound mice, APC$^{-/-}$; FASN$^{-/-}$ and APC$^{-/-}$; KHK$^{-/-}$ mice, were generated by crossing the APC$^{-/-}$ line with *FASN*$^{flox/flox}$ mice and mice deficient in ketohexokinase (KHK). *FASN*$^{flox/flox}$ mice were generously provided by Dr. Semenkovich at Washington University (*31*). KHK$^{-/-}$ mice lacking both KHK-A and KHK-C in C57BL/6 background and were kindly shared by Dr. Bonthron at University of Leeds at UK and Drs. Lanaspa and Johnson at University of Colorado (*33*). *CDX2P-CreER^{T2}* mice were purchased from JAX stock #022390 (*15*) and crossed to *APC$^{flox/flox}$* mice to generate *CDX2P-CreER^{T2}*; *APC$^{flox/flox}$* mice. We used only male mice throughout the study to reflect the strong epidemiological evidence linking obesity or sugar consumption to colon cancer incidence in male but not female (*37*). Mice were maintained in temperature- and humidity-controlled specific pathogen-free conditions on a 12-hour light/dark cycle and received rodent chow (PicoLab Rodent 20 5053 lab Diet St. Louis, MO) and free access to drinking water. Mice harboring *Lgr5-EGFP-IRES-creERT2* allele (APC$^{-/-}$, APC$^{-/-}$; FASN$^{-/-}$ and APC$^{-/-}$; KHK$^{-/-}$) were injected a single tamoxifen intraperitoneal injection (IP) (20 mg/kg, Sigma, Cat. #T5648) at 7 to 8 weeks of age to induce tumors. *CDX2P-CreER^{T2}*; *APC$^{flox/flox}$* mice were injected a single tamoxifen IP injection (16 mg/kg) at 7 to 8 weeks of age. Littermates without tumor induction were used as wild-type (WT) controls. High-fructose corn syrup (HFCS) was prepared by combining D-(+)-Glucose (Sigma, Cat. #G8270) and D-(-)-Fructose (Sigma, Cat. #F0127) in a 45:55 ratio using tap water. Age-matched cohorts of WT and APC$^{-/-}$ were treated with HFCS by two types of methods. The first is via *ad libitum* delivery in the drinking water (25% HFCS in water, referred as the Water Bottle or WB group). The other method is via daily oral gavage of HFCS (Glucose 45 mg + Fructose 55 mg, total 400 ul in tap water, referred as HFCS group). As a control for the HFCS group, mice were treated with 400 ul of tap water via daily oral gavage (referred as Con group). APC$^{-/-}$; KHK$^{-/-}$ mice were treated with HFCS or water via daily oral gavage (HFCS or Con groups). Treatments in APC$^{-/-}$ and APC$^{-/-}$; KHK$^{-/-}$ mice started the day after tamoxifen injection. Mice were longitudinally assessed for intestinal tumor progression by testing weekly for the presence of heme in the stool using the Hemocult Sensa test (Beckman Coulter). Animals were euthanized based on the degree weight loss and the Hemocult score. This resulted in all APC$^{-/-}$, APC$^{-/-}$; FASN$^{-/-}$, and APC$^{-/-}$; KHK$^{-/-}$ mice being sacrificed between 8 and 9 weeks after treatment. Polyp number and volume were determined in whole mount tissue following methylene blue staining (0.2% methylene blue in H_2O, Sigma, Cat. #M9140) using a dissecting microscope in a blinded manner. Subsequently, intestines were Swiss-rolled, paraffin embedded, and subjected to histologic analysis following H&E staining. Experiments were repeated multiple times over 15 cohorts of 8-10 mice per group. All animal studies were approved by the Institutional Animal Care and Use Committee (IACUC) of Weill Cornell Medical College and Baylor College of Mecicine.

Body composition and glucose tolerance

Body Mass, Fat mass (FM) and fat-free mass (FFM) were measured and calculated using magnetic resonance spectroscopy (MRI) as previously described (*38*). Skeletal muscle was assessed by measuring the weight of the gastrocnemius. Visceral fat was assessed by measuring the weight of the gonadal white adipose depot. Glucose tolerance testing was performed in WT and APC$^{-/-}$ mice with or without chronic treatment using WB or HFCS. Mice were fasted for six hours after which 2 g/kg intraperitoneal glucose solution was administered. Tail blood glucose was measured with a glucose meter over time. Mice were allowed to recover and resume their diets after completion of the testing.

Biochemical analysis

The serum level of insulin was determined using the Ultra Sensitive Mouse Insulin ELISA Kit (Crystal Chem Inc. Cat. #90080) after mice were fasted for six hours. Glucose and Fructose concentration in the serum and the intestinal lumen were measured with EnzyChrom glucose assay kit (BioAssay Systems, Cat. #EBGL-100) and EnzyChrom fructose assay kit (BioAssay Systems, Cat. #EFRU-100). For measurement of hepatic and stool triglyceride, the frozen liver or stool were weighed and digested in 6 volumes of alcoholic KOH (2:1 EtOH to 30% KOH) at 60°C

until tissue was completely dissolved. 500µL of digest was added to 540µL of 1M $MgCl_2$ and mixed well. After 10-minute incubation on ice, samples were centrifuged for 30 minutes at maximum speed. The supernatant was aspirated into a new tube and glycerol content was measured using calorimetric assay (Stanbio, Boerne, TX). Phosphofructokinase activity was measured using a commercial assay kit (Abcam ab155898). As per the vendor's instructions, tumors were homogenized by Dounce homogenizer in ice-cold assay buffer. We determined that 5ug of tumor homogenate was ideal per reaction. The kinetic change in absorbance was measured using a POLARstar Omega plate reader.

Metabolite extraction for targeted metabolomics

Polar metabolites were extracted from the frozen liver, small intestinal epithelium, and tumor tissue using either 80% methanol(*39*) or a 40:40:20 mixture of acetonitrile:methanol:water with 0.1M formic acid followed by neutralization with ammonium bicarbonate for ATP measurements (*40*). Briefly, each sample was crushed on dry ice using a mortar and pestle and transferred to a pre-cooled 2 mL homogenization tube. Pre-cooled extraction buffer (1 mL) was added to each sample and incubated on ice for 10min. Samples were then centrifuged at 4 °C for 15 minutes at 14,000 rpm. The supernatants were removed and pellets were re-extracted with 0.5 mL of extraction buffer. The pooled supernatants were then evaporated, and used for LC/MS. For fatty acid analysis, total tissue lipids were extracted and saponified using previously described methods(*41*). Lipids were extracted from crushed tissue powder using 1ml of cold 50:50 methanol:water containing 0.1M HCl followed by the addition of 0.5ml of chloroform. The mixture was vortexed and centrifuged at 16,000xg for 5min. The lower chloroform layer was transferred to a glass vial and pooled together with a subsequent 0.5ml chloroform wash of the methanol:water phase. The chloroform phase was dried under nitrogen gas, resuspended in 1ml of 90:10 MeOH:H20 containing 0.3M KOH, and incubated for 1h at 80°C to saponify fatty acids. The fatty acids were then extracted in 1ml of hexanes, dried under nitrogen gas, and used for LC/MS.

Targeted metabolomics analysis

Analytical mass spectroscopy was carried out to quantify aqueous polar metabolites, fatty acids, and sugarphosphates. For polar metabolites, aqueous tissue extracts were separated via liquid chromatography on an Agilent 1290 LC system (Agilent Technologies, Santa Clara, CA) as detailed elsewhere (*42*). Briefly, solvent A (ddH_2O with 0.2% formic acid) and solvent B (acetonitrile with 0.2% formic acid) mobile phase solvents are paired to a Cogent Diamond Hydride Type C column (MicroSolv Technology Corp, Leland, NC) with the following gradient applied at 0.4 mL/min flow rate: 0–2 min, 85% B; 3–5 min, 80% B; 6–7 min, 75%; 8–9 min, 70% B; 10–11.1 min, 50% B; 11.1–14 min 20% B; 14.1–24 min 5% B followed by a 10 min wash period at 85% B. The continuous infusion of twin reference masses for mass axis calibration achieved mass errors of <6 ppm.

Dried fatty acid pellets were resuspended in 50% methanol and 0.2% formic acid in ddH_2O and transferred to glass autosampler vials. Mass spectrometry was based on a previously established method (*43*). Briefly, a ZORBAX Eclipse Plus C18 column 4.6 mm × 100 mm, 3.5 µm (Agilent Technologies, Santa Clara, CA) was paired with an Agilent 1200 Rapid Resolution system. The LC parameters were as follows: column temperature, 40°C; injection volume, 4 µL; flow rate of 0.4 mL/min. Chromatography relied on a gradient of solvent A (0.2% formic acid in methanol) to solvent B (0.2% formic acid in ddH_2O), where a 2-minute equilibration period of 90% A was followed by a linear decrease over the course of 18-minutes to 2% followed by a 17-minute hold. Acquisition was performed on an Agilent 6224 TOF mass spectrometer in high resolution mode. The following settings were used: ESI capillary voltage, 4000 V (+) and 3500 V (−); fragmentor 170 V, the liquid nebulizer was set to 35 psig and the nitrogen drying gas was set to a flow rate of 12 L/min at 250 °C. APCI capillary voltage was set at 4000 V (both ion modes), corona current was set to 4 µA and fragmentor at 170 V. The liquid nebulizer was set to 60 psig. Centroid mode was used for acquisition of 1.4 spectra/s for m/z's from 50–1300.

Identification of sugar phosphates benefitted from the recent development of an ion pairing chromatographic method that was developed for the resolution of phosphate-containing compounds from small molecule extracts (*44*). Reproducible separation of individual hexose phosphate species was accomplished on an Agilent 1290 Infinity LC system by injection of 5 µL of filtered extract through an Agilent ZORBAX Extend C18, 2.1 × 150 mm, 1.8 µm (Agilent Technologies, Santa Clara, CA) downstream of an Agilent ZORBAX SB-C8, 2.1 mm × 30 mm, 3.5 µm

(Agilent Technologies, Santa Clara, CA) guard column heated to 40°C. Solvent A (97% water/ 3% methanol containing 5 mM tetrabutylammonium hydroxide (TBA) and 5.5 mM acetic acid) and Solvent B (methanol containing 5 mM TBA and 5.5 mM acetic acid) were infused at a flow rate of 0.250 mL/min. The 24-minute reverse phase gradient was as follows: 0–3.5 min, 0% B; 4-7.5 min, 30% B; 8-15 min, 35% B; 20-24 min, 99% B; followed by a 7-minute post-run at 0% B. Acquisition was performed on an Agilent 6230 TOF mass spectrometer (Agilent Technologies, Santa Clara, CA) employing an Agilent Jet Stream electrospray ionization source (Agilent Technologies, Santa Clara, CA) operated at 4000 V Cap and 2000 V nozzle voltage in high resolution, negative mode. The following settings were used for acquisition: The sample nebulizer set to 45 psig with sheath gas flow of 12 L/min at 400°C. Drying gas was kept at 325°C at 8 L/min. Fragmentor was set to 125 V, with the skimmer set to 50 V and Octopole Vpp at 400 V. Samples were acquired in centroid mode for 1.5 spectra/s for m/z's from 50–1100.

Collected data from the above methods was analyzed by batch processing with Agilent MassHunter Profinder software version 8.0SP1 (Agilent Technologies, Santa Clara, CA) for both targeted and untargeted analysis. Targeted metabolites were identified from m/z pairs by both retention time comparability with authentic standards and expected isotopomer distributions. Untargeted compounds were first identified as m/z:RT pairs using the Profinder Batch Targeted Feature Extraction. Candidate pairs were then processed through Agilent Mass Profiler Professional software version B14.5 (Agilent Technologies, Santa Clara, CA), where features were assessed for quality control measures (threshold m/z value peak height >10,000, coefficient of variation <25%) and statistically analyzed. When indicated mice or tumors were pre-treated with D-[^{14}C(U)]-Glucose (Perkin Elmer, Waltham, MA), D-[^{14}C(U)]-Fructose (American Radiolabeled Chemicals, St. Louis, MO), D-[U-^{13}C6]-Glucose (Cambridge Isotope Laboratories, Tewksbury, MA), or D-[U-^{13}C6]-Fructose (Cambridge Isotope Laboratories, Tewksbury, MA). The various fatty acids are represented by "Cx:y" where x denotes the number of carbons and y the number of double bonds. For example, the symbol for palmitic acid is C16:0 and palmitoleic acid is C16:1. Eicosanoids were measured from total tumor lysates using the Comprehensive Eicosanoid Panel at the UCSD Lipidomics Core (*45*).

Untargeted metabolites profiling

The excised animal tissues or tumors were added to 2 mL Eppendorf tubes containing 600 µL of 3 mM monobrombimane (MBB) in CH_3OH:H_2O (80:20) at -20°C and incubated for 2 h, followed by 1 h incubation at 0°C. Here, MBB was used to react with thiols and protect them for further oxidation. This initial incubation was followed by tissue disruption using stainless steel beads in a TissueLyser (Qiagen) and an additional 30 min at -20°C. Extracts were centrifuged for 15 min at 13000 rpm to pellet insoluble material and supernatants were transferred to clean tubes. This extraction was repeated two additional times and all three supernatants were dried in a speed-vac (Savant) and stored at −80 °C until analysis. For normalization of sample analyses, post-extracted tissue/tumor pellets were solubilized in 800 µL of 0.2 M aqueous NaOH at 95 °C for 60 min and the pellet protein was determined using the BioRad assay, relative to bovine serum albumin standards (0–1.5 mg/mL). For metabolite analysis, dried tissue/tumor extracts were reconstituted in CH_3CN:H_2O (70:30) containing 0.025% acetic acid at a relative protein concentration of 10 µg/µL and 3 µL solution was injected for LC/MS. Plasma were incubated with 2.5 mM MBB in CH_3OH:H_2O (80:20) at room temperature for 30 min, then diluted with same volume of CH_3CN:H_2O (70:30) containing 0.025% acetic acid. The diluted samples were briefly vortexed and centrifuged for 25 min at 20,000g to pellet precipitated proteins. The supernatants were transferred to autosampler vials with 3 µL solution injection for analysis by TOF LC/MS.

Metabolite profiling was performed using an Agilent Model 1200 liquid chromatography system coupled to an Agilent Model 6230 time-of-flight mass analyzer as described previously (*11*). Chromatography of metabolites was performed using aqueous normal phase (ANP) gradient separation on a Diamond Hydride column (Microsolv, NJ). The mobile phases consisted of 6 µM edta and 0.025% acetic acid in isopropanol:H_2O (50:50) (solvent A) and 6 µM edta and 5mM ammonium acetate in CH_3CN: H_2O (90:10) (solvent B). The following gradient was applied: 0–1.0 min, 99% B; 1.0–15.0 min, to 20% B; 15.1–29.0 min, 0% B; 29.1-37 min, 99% B. Both positive and negative mass spectra were acquired in 2 GHz (extended dynamic range) mode with 1.41 spectra/sec sampled over a mass/charge range of 40–1400 Daltons. Data was saved in both centroid and profile mode using Agilent Mass Hunter Workstation B600 Data acquisition Software.

Raw data files were analyzed using Mass Profiler Professional (Agilent, version B14.5) and Mass Hunter Profinder (version B08.00). Briefly, the molecular feature extraction (MFE) searches compounds based on the profile of identical m/z values and retention times, within a defined mass accuracy (<5 ppm). These features are further grouped into one or more "compounds" based on their isotope pattern, the formation of dimer, adduct ions (e.g. H^+, Na^+, NH_4^+ for positive mode and H^-, CH_3COO^-, $HCOO^-$ and Cl^- for negative mode) and common neutral losses of H_2O and NH_3. The identified features were manually validated following extraction. The identification is further confirmed by comparison to chemical standards.

Immunoblotting and immunohistochemistry

Liver, small intestine epithelium, and tumor tissue were lysed using lysis buffer containing 50 mM Tris·HCl (pH 7.4), 150mM NaCl, 1mM EDTA, 10% glycerol, 1% NP-40, 0.5% Triton X-100, and 1 tablet (per 10mL) of protease and phosphatase inhibitor. Protein extracts (50 µg) were separated by 4–12% NuPAGE Bis-Tris gel (Invitrogen, Carlsbad, CA) and transferred to 0.45µm PVDF membranes with wet transfer cells (Bio-Rad Laboratories, Hercules, CA). After 1 h of blocking with Tris-buffered saline with 0.1% (v/v) Tween 20 (TBST) containing 5% (w/v) BSA, membranes were incubated overnight at 4° C with antibodies against GLUT1 (Millipore 07-1401), GLUT2 (abcam ab192599), GLUT5 (abcam ab113931), SGLT1 (abcam ab14686), HK1 (CST 2024), HK2 (CST 2867), KHK (abcam ab154405), ALDOA (CST8060), ALDOB (abcam ab152828), ALDOC (proteintech 14884-1-AP), PKL (abcam ab171744), PKM1 (CST 7067), PKM2 (CST 4053), ENO1 (CST 3810) at a 1:1000 dilution in 5% BSA followed by a TBST wash and the appropriate secondary antibody (1:3000) for 1h at room temperature. The signals were detected on HyBlot CL Autoradiography Film (Denville Scientific Holliston, MA) with SuperSignal Western Blot enhancer solution (Thermo Fisher, Waltham, MA). GLUT5 immunohistochemistry on Tumor Microarray (US Biomax Inc. Cat. #BC05002a) was done using the VENTANA BenchMark ULTRA stainer. Slides were deparaffinized with xylene and rehydrated in a graded ethanol series and water. Antigen retrieval was performed with 0.01 M citrate, pH 6.0 buffer by heating the samples in the microwave for 15 min. Sections were blocked with avidin/biotin blocking for 30 minutes. Sections were incubated with anti- SLC2A5 (Sigma, Cat. # AV42096, dilution 1:150) for 1 hour, followed by 60 minutes incubation with biotinylated goat anti-rabbit IgG (Vector labs, Cat. # PK6101, dilution 1:500). The detection was performed with the DAB detection kit (Ventana Medical Systems) according to manufacturer's instructions, followed by counterstaining with hematoxylin (Ventana Medical Systems) and cover slipping with Permount (Fisher Scientific).

Transcriptome profiling using RNA-seq

Total RNA was extracted from small intestine epithelium and tumor tissue using RNeasy kit (Qiagen). 500 ug of total RNA of each sample was submitted to the Weill Cornell Medicine Genomics Resources Core Facility. Following isolation, total RNA integrity is checked using an Agilent Technologies 2100 Bioanalyzer with an RNA Integrity Number (RIN) value greater than 8. The library construction was followed by the protocol from Illumina TruSeq Stranded mRNA Sample Preparation kit. After the cBot has generated clonal clusters of the DNA fragments, they were sequenced using HiSeq4000 using Paired End Clustering and 50x2 Cycles Sequencing (per lane). The quality of the raw FASTQ files were checked with FastQC, then mapped to mouse reference GRCm38 using STAR (v3.5.3a) (*46*). FPKM (Fragments per Kilobase per million) was estimated using Cufflinks (v2.2.1) and HTSeq (v0.6.1) (*47*, *48*). Mouse gene symbols were converted to human gene symbols using the vertebrate homology list provided by Mouse Genome Informatics(*49*). Differential expression analyses and variance stabilizing transformation for unsupervised analyses were performed using DESeq2 (v1.14.1)(*50*). All custom code, statistical analysis, and visualizations were performed in Python or R, and used Nextflow to manage the computational pipelines(*51*). Code used for these analyses are available here: https://github.com/murphycj/manuscripts/tree/master/GoncalvesEtAl2018.

Lipid incorporation from glucose

For *in vivo* measurement of glucose incorporation into lipids, mice were given a one-time bolus of HFCS (Glucose 45 mg + Fructose 55 mg, total 400 ul in tap water) containing 5 µCi of D-[^{14}C(U)]-Glucose (Perkin Elmer, Waltham, MA). Four hours after the bolus, the mice were euthanized and the small intestine epithelium and tumor tissue were

harvested and flash frozen in liquid nitrogen. Lipids were extracted and dried as described above using chloroform and methanol. The dried lipid extract was suspended in 4 mL of Ultima Gold liquid scintillation cocktail (PerkinElmer, Waltham, MA) and radioactivity was measured in disintegrations per minute (DPM) using a Tri-carb 2910 TR Liquid Scintillation Counter (PerkinElmer, Waltham, MA). Values were normalized to tissue mass.

RT-PCR

Total RNA was extracted from small intestine epithelium and tumor tissue using Trizol (Thermo Fisher, Waltham, MA) followed by clean-up using RNeasy kit (Qiagen, Hilden, Germany). One microgram of total RNA was reversed transcribed using SuperScript VILO Master Mix (Thermo Fisher, Waltham, MA). Quantitative real time PCR was done using the Applied Biosystems TaqMan Gene Expression Assays (Thermo Fisher, Waltham, MA) with the following primers: ACACA (Mm01304257_m1), FASN, (Mm00662319_m1), SCD1 (Mm00772290_m1), and ACTB (Mm00607939_s1). The relative expression of each gene was calculated after normalizing to ACTB endogenous control and using the comparative ΔC_t method.

ATP measurement in tumors by HPLC

Polar metabolites were extracted from the tumor tissue using a 40:40:20 mixture of acetonitrile:methanol:water with 0.1 M formic acid followed by neutralization with ammonium bicarbonate (*40*). The dried extracts were then dissolved in 100 µl of 0.1 M KH_2PO_4 (pH 6.0) buffer and used in an ion-pair reversed-phase high-performance liquid chromatography (HPLC) method that was adapted from a previously published method (*52*). Five microliters of dissolved extract was injected into an Agilent 1260 binary pump connected to a C18 column (Phenomenex, 150 mm x 4.6 mm, 5 µm; LUNA) with a 1 mL/min flow rate. ATP and ADP were separated using an isocratic mobile phase of 0.1 M KH_2PO_4 (pH 6.0) and absorbance was monitored by a diode array detector. Peaks were quantified at A_{254} using Chemstation software (Agilent Technologies, Santa Clara, CA).

Statistics

All summary data are expressed as mean ± SEM. When comparing means from two groups, a two-tailed, unpaired *t*-test was used following confirmation that the data was sampled from a Gaussian distribution by the D'Agostino-Pearson normality test. When comparing effects of genotype and treatment, a two-way ANOVA was done with post-test comparisons made by the Holm multiple comparisons test using Prism 6 (GraphPad La Jolla, CA). Statistical significance is indicated in figures using the following denotation: **P*<0.05, ***P*<0.01, ****P*<0.001, and *****P*<0.0001.

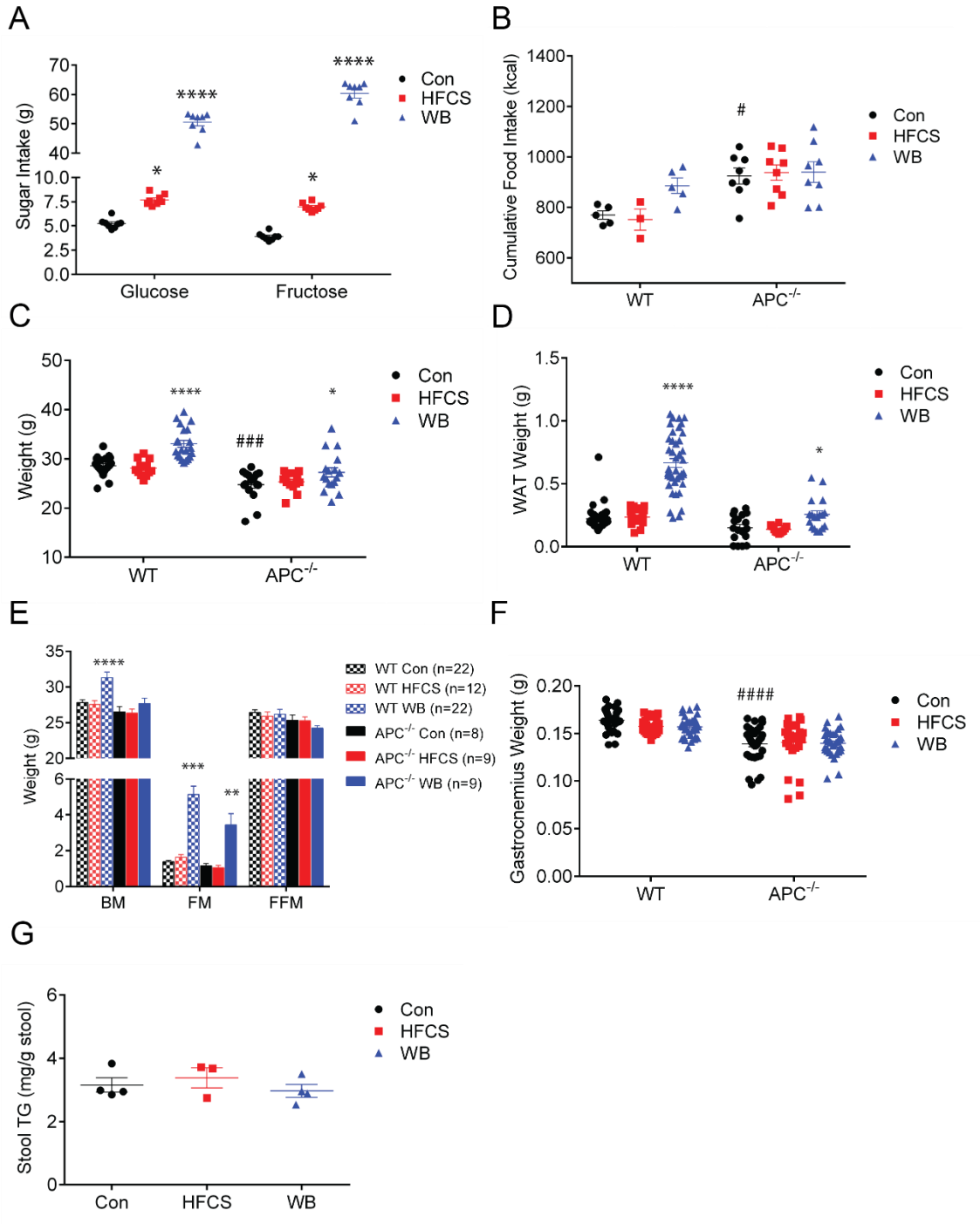

fig. S1. Changes in body composition and food intake following treatment with high-fructose corn syrup.

(A) Cumulative sugar (glucose and fructose) intake was calculated by combining the consumption of sugar in the normal chow diet with supplemental HFCS (via a daily oral bolus by gavage or *ad libitum* access via the water bottle, WB) over 8 weeks in APC$^{-/-}$ mice. Sugar consumption in both APC$^{-/-}$ and WT mice increased by a factor of 10 in comparison to mice fed normal chow diet with non-sugared water (Con group) over an 8-week period. n=8 per group. Two-way ANOVA followed by Holm-Sidak post-test. *P<0.05, ****P<0.0001 (B) Cumulative food intake over 8 weeks of treatment in wild-type (WT) and tumor-bearing mice (APC$^{-/-}$) mice following 8 weeks of treatment with water (Con), a daily oral gavage of high-fructose corn syrup (HFCS), and mice supplied with unlimited high-fructose corn syrup via the water bottle (WB). Con, HFCS, and WB groups was calculated by

measuring normal chow consumption plus supplemental HFCS (via daily oral gavage or WB). WT Con (n=5), HFCS (n=3), and WB (n=5). $APC^{-/-}$ (n=8 per group). Two-way ANOVA with Holm-Sidak post-test comparing HFCS and WB to Con showed no differences, comparisons between $APC^{-/-}$ Con to WT Con $^{\#}P<0.05$. (C) Final body weight in WT and $APC^{-/-}$mice following 8 weeks of treatment with Con, HFCS, and WB. Although there were no differences in cumulative food intake in the WB versus Con groups, the high intake of HFCS (approximately 48% of total daily calorie intake) significantly increased body weight. WT Con (n=22), HFCS (n=12), and WB (n=21). $APC^{-/-}$ Con (n=17), HFCS (n=13), and WB (n=17). Two-way ANOVA with Holm-Sidak post-test comparing HFCS and WB to Con (*), and $APC^{-/-}$ Con to WT Con (#) $^{*}P<0.05$, $^{\#\#\#}P<0.001$, $^{****}P<0.0001$. (D) Gonadal white adipose tissue weight (WAT) in WT and $APC^{-/-}$mice following 8 weeks of treatment with Con, HFCS, and WB. WT Con (n=22), HFCS (n=12), and WB (n=10). $APC^{-/-}$ Con (n=9), HFCS (n=6), and WB (n=9). Two-way ANOVA with Holm-Sidak post-test comparing HFCS and WB to Con (*), and $APC^{-/-}$ Con to WT Con (no significant changes) $^{*}P<0.05$, $^{****}P<0.0001$. (E) Body mass (BM), fat mass (FM), and fat-free mass (FFM) in WT and $APC^{-/-}$mice following 8 weeks of treatment with Con, HFCS, and WB. WT Con (n=22), HFCS (n=12), and WB (n=22). $APC^{-/-}$ Con (n=8), HFCS (n=9), and WB (n=9). Two-way ANOVA with Holm-Sidak post-test comparing HFCS and WB to Con (*), and $APC^{-/-}$ Con to WT Con (no significant changes) $^{**}P<0.01$, $^{***}P<0.001$ $^{****}P<0.0001$. (F) Gastrocnemius weight in WT and $APC^{-/-}$mice following 8 weeks of treatment with Con, HFCS, and WB. WT Con (n=17), HFCS (n=12), and WB (n=16). $APC^{-/-}$ Con (n=17), HFCS (n=14), and WB (n=17). Two-way ANOVA with Holm-Sidak post-test comparing HFCS and WB to Con showed no differences, comparisons between $APC^{-/-}$ Con to WT Con $^{\#\#\#\#}P<0.0001$. (G) Stool triglyceride (TG) in $APC^{-/-}$mice following 8 weeks of treatment with Con, HFCS, and WB. $APC^{-/-}$ Con (n=4), HFCS (n=3), and WB (n=4). One-way ANOVA (no significant changes). All data represent means ± S.E.M.

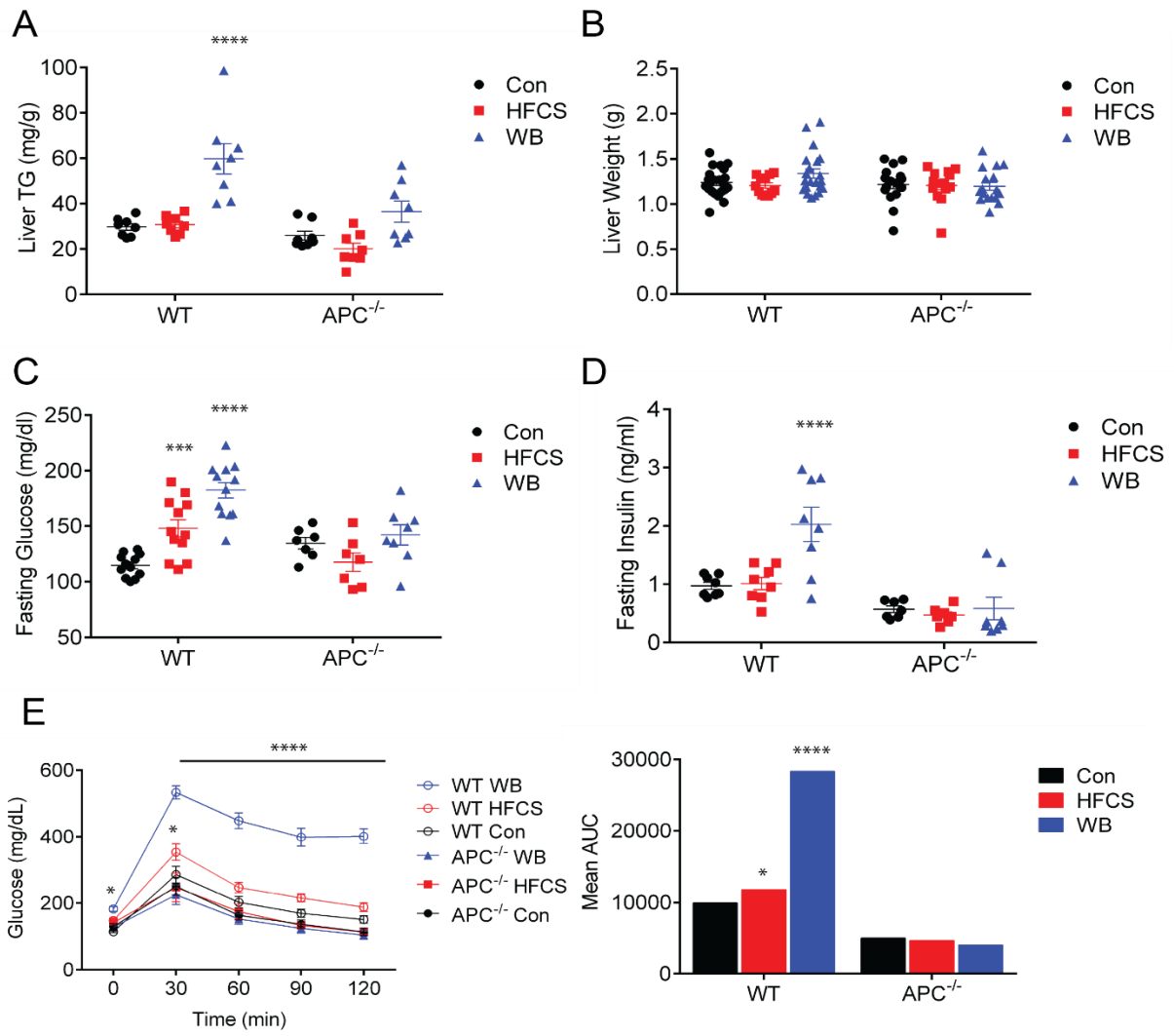

fig. S2. Changes in systemic glucose metabolism following treatment with high-fructose corn syrup in WT and tumor-bearing APC$^{-/-}$ mice.

(A) Liver triglyceride (TG) in wild-type (WT) and tumor-bearing mice (APC$^{-/-}$) following 8 weeks of treatment with water (Con), a daily oral gavage of high-fructose corn syrup (HFCS), and mice supplied with unlimited high-fructose corn syrup via the water bottle (WB). n=8 per group. Two-way ANOVA with Holm-Sidak post-test comparing HFCS and WB to Con (*), and APC$^{-/-}$ Con to WT Con (no significant changes) ****P<0.0001 (B) Liver weight in WT and APC$^{-/-}$mice following 8 weeks of treatment with Con, HFCS, and WB. WT Con (n=22), HFCS (n=12), and WB (n=21). APC$^{-/-}$ Con (n=17), HFCS (n=14), and WB (n=17). Two-way ANOVA with Holm-Sidak post-test with no significant changes (C) Fasting serum glucose in WT and APC$^{-/-}$mice following 8 weeks of treatment with Con, HFCS, and WB. WT n=12 per group. APC$^{-/-}$ Con (n=7), HFCS (n=7), and WB (n=8). Two-way ANOVA with Holm-Sidak post-test comparing HFCS and WB to Con (*), and APC$^{-/-}$ Con to WT Con (no significant changes) ***P<0.001, ****P<0.0001 (D) Fasting serum insulin in WT and APC$^{-/-}$ mice following 8 weeks of treatment with Con, HFCS, and WB. WT n=8 per group. APC$^{-/-}$ Con (n=7), HFCS (n=7), and WB (n=8). Two-way ANOVA with Holm-Sidak post-test comparing HFCS and WB to Con (*), and APC$^{-/-}$ Con to WT Con (no significant changes) ****P<0.0001 (E) Serum glucose (left) following intraperitoneal injection of 2 mg/kg glucose in WT and APC$^{-/-}$mice following 8 weeks of treatment with Con, HFCS, and WB. Mean area under the curve (AUC, right). WT n=12 per group. APC$^{-/-}$ Con (n=9), HFCS (n=6), and WB (n=9). Two-way ANOVA with Holm-Sidak post-test comparing HFCS and WB to Con, *P<0.05, ****P<0.0001. Interestingly, APC$^{-/-}$ mice were protected from HFCS-induced metabolic dysfunction. All data represent means ± S.E.M.

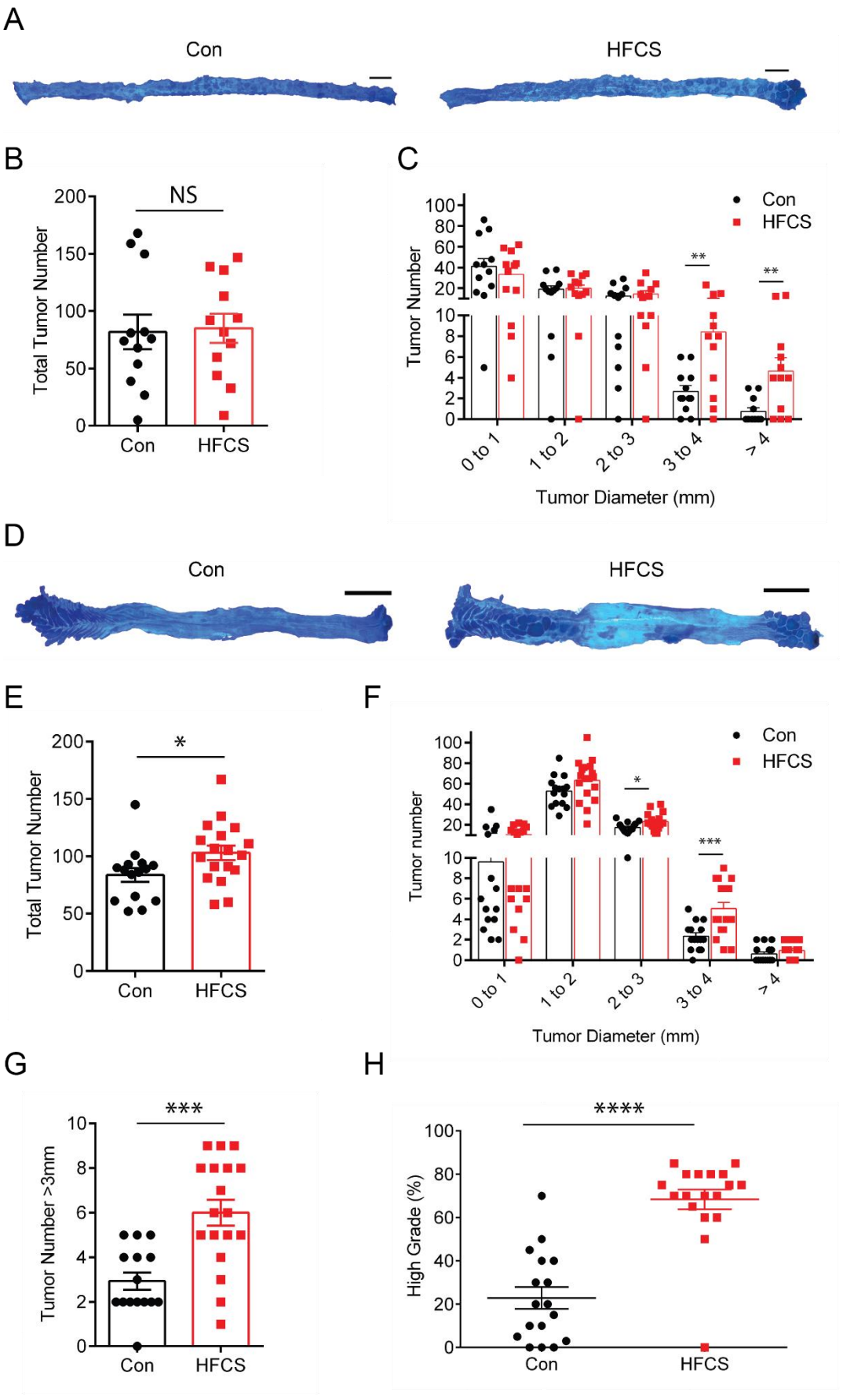
A
Con
HFCS
B
NS
Total Tumor Number
200
150
100
50
0
Con
HFCS
C
Con
HFCS
Tumor Number
100
80
60
40
20
10
8
6
4
2
0
**
**
0 to 1
1 to 2
2 to 3
3 to 4
> 4
Tumor Diameter (mm)
D
Con
HFCS
E
*
Total Tumor Number
200
150
100
50
0
Con
HFCS
F
Con
HFCS
Tumor number
100
80
60
40
20
10
8
6
4
2
0
*
***
0 to 1
1 to 2
2 to 3
3 to 4
> 4
Tumor Diameter (mm)
G
***
Tumor Number >3mm
10
8
6
4
2
0
Con
HFCS
H
****
High Grade (%)
100
80
60
40
20
0
Con
HFCS

fig. S3. Increased tumor size but not total number following high-fructose corn syrup treatment for 8 weeks

(A) Representative images of the distal small intestine in $APC^{-/-}$ mice following daily oral gavage of water (Con) or high-fructose corn syrup (HFCS) for 8 weeks. Tissue is shown in whole-mount after methylene blue staining. Black bar indicates 1cm (B) Total number of tumors in Con and HFCS treated $APC^{-/-}$ mice. n=12 per group. Student's t-test. NS: not significant. (C) The size of each tumor (diameter) in the intestine was determined in whole-mount tissue after methylene blue staining, using a dissecting microscope. Data presented is the tumor size distribution in Con and HFCS treated $APC^{-/-}$ mice. n=12 per group. Con vs HFCS compared by t-test with correction for multiple comparisons using Holm-Sidak method $^{**}P<0.01$. (D) Representative images of the colon in *CDX2P-CreER*^{T2}; *APC*$^{flox/flox}$ (CDX2-$APC^{-/-}$) mice following daily oral gavage of Con or HFCS for 8 weeks. Tissue is shown in whole-mount after methylene blue staining. Black bar indicates 1cm. (E) The size of each tumor (diameter) in the intestine was determined in whole-mount tissue after methylene blue staining, using a dissecting microscope. Data presented is the total number of tumor in Con and HFCS treated CDX2-$APC^{-/-}$ mice. Con (n=15), HFCS (n=18). Student's t-test. $^{*}P<0.05$, (F) The size of each tumor (diameter) in the intestine was determined in whole-mount tissue after methylene blue staining, using a dissecting microscope. Data presented is the tumor size distribution in Con and HFCS treated CDX2-$APC^{-/-}$mice. Con (n=15), HFCS (n=18), Con vs HFCS compared by t-test with correction for multiple comparisons using Holm-Sidak method $^{*}P<0.05$, $^{***}P<0.001$, (G) Number of tumors over 3 mm in diameter in Con and HFCS treated CDX2-$APC^{-/-}$ mice. Con (n=15), HFCS (n=18), Student's t-test. $^{***}P<0.001$. (H) Percent of high grade lesions from the intestine of Con and HFCS treated CDX2-$APC^{-/-}$ mice. Con (n=17), HFCS (n=18), Student's t-test. $^{****}P<0.0001$. All data represent means ± S.E.M.

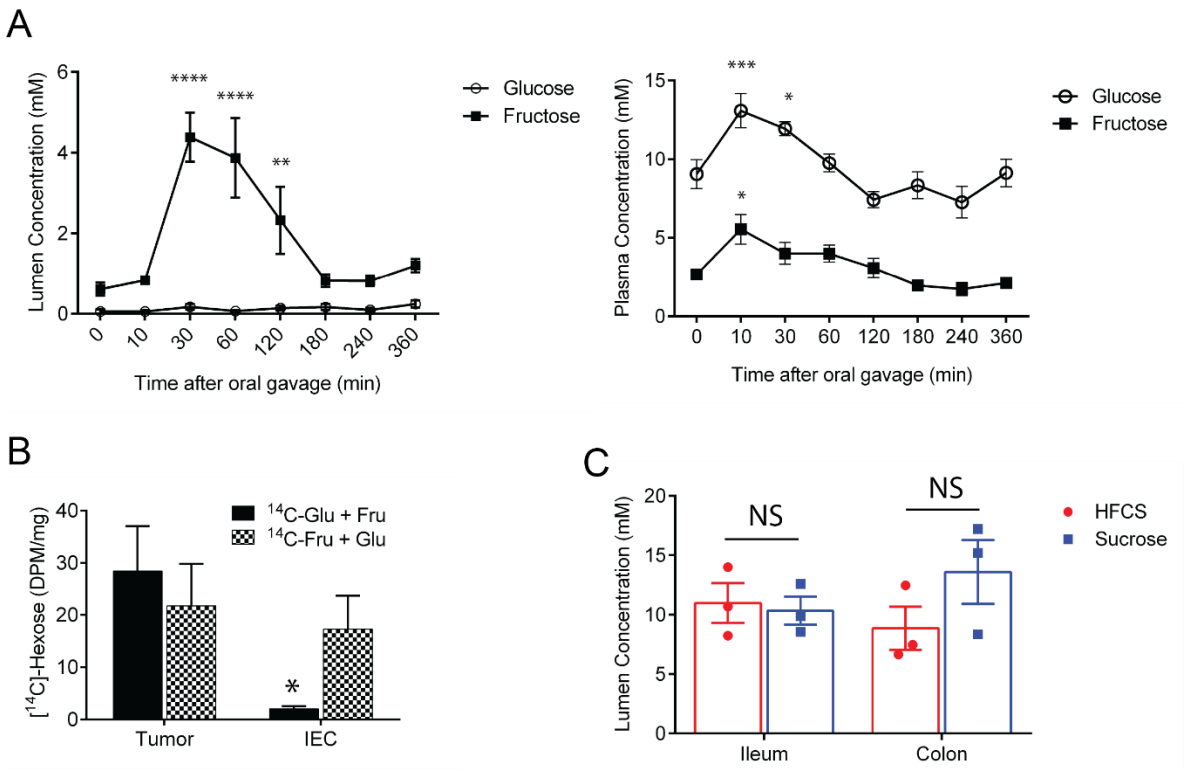

fig. S4. Tumors directly take up fructose and glucose in the intestinal lumen and serum, respectively following a bolus of HFCS treatment via oral gavage.

(A) Glucose and fructose concentration in the colonic lumen (left) and serum (right) over time in wild-type (WT) mice (C57BL/6J) following a single oral gavage bolus of HFCS. n=5 per group. Two-way ANOVA with Holm-Sidak post-test comparing time 0 to subsequent times. **P*<0.05, ***P*<0.01, ****P*<0.001, *****P*<0.0001. (B) The amount of radioactivity present in $APC^{-/-}$ tumors and intestinal epithelial cells (IEC) 30 min after an oral gavage bolus with U-[^{14}C]-labeled glucose (^{14}C-Glu) or U-[^{14}C]-labeled fructose (^{14}C-Fru) in the presence of glucose (Glu) or fructose (Fru) as indicated. Radioactivity amount is presented as disintegrations per minute (DPM) per microgram of protein input. n=5 per group. Two-way ANOVA with Holm-Sidak post-test comparing tumor to IEC, **P*<0.05. (C) Fructose concentration in the ileum and colonic lumen 90 min following an oral gavage bolus of equimolar HFCS (100 mg glucose + 100 mg fructose) or sucrose (200 mg). Both HFCS and sucrose treatment via oral gavage give similar levels of fructose in the lumen of the ileum and the colon. n=3 per group. Comparisons were made using t-test with correction for multiple comparisons using Holm-Sidak method. NS, not significant. All data represent means ± S.E.M.

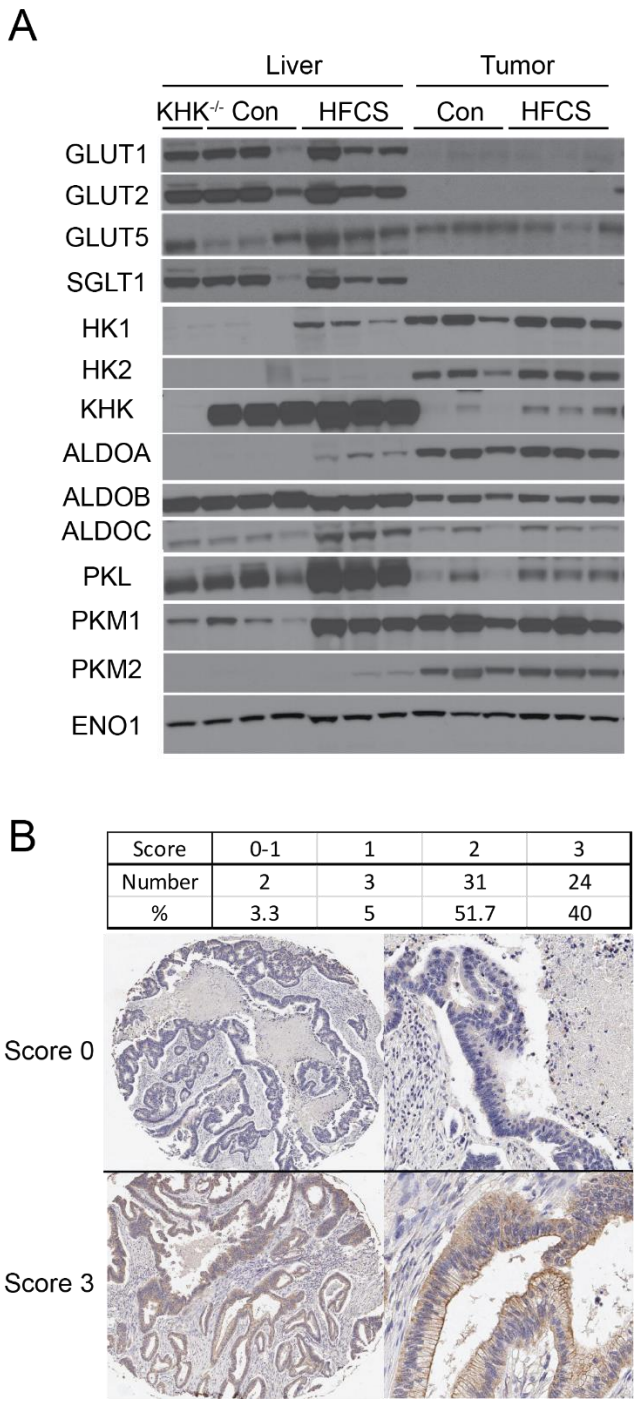

Score	0-1	1	2	3
Number	2	3	31	24
%	3.3	5	51.7	40

fig. S5. Immunoblot of key glycolysis and fructolysis proteins from the mouse tissues.

(A) The liver from a WT KHK$^{-/-}$ mouse and the liver and tumor tissue from APC$^{-/-}$ mice treated with a daily oral gavage of water (Con) or high-fructose corn syrup (HFCS) for 8 weeks were removed, homogenized, and subjected to immunoblot. GLUT1, Glucose transporter 1; GLUT2, Glucose transporter 2; GLUT5, Glucose transporter 5; SGLT1, Sodium/glucose cotransporter 1; HK1, Hexokinase 1; HK2, Hexokinase 2; KHK, Ketohexokinase; ALDOA, Adolase A; ALDOB, Adolase B; ALDOC, Aldolase C; PKL, Pyruvate Kinase Liver Isozyme; PKM1, Pyruvate Kinase Muscle Isozyme isoform 1; PKM2, Pyruvate Kinase Muscle Isozyme isoform 2; and ENO1, enolase 1, as a control between tissues. (B) Glut5 immunohistochemical staining and quantification of human colorectal tumors from a tumor tissue microarray containing various stages of colorectal cancer from adenoma, adenocarcinoma and metastatic colon cancer. Scoring performed in a blinded fashion by pathologist.

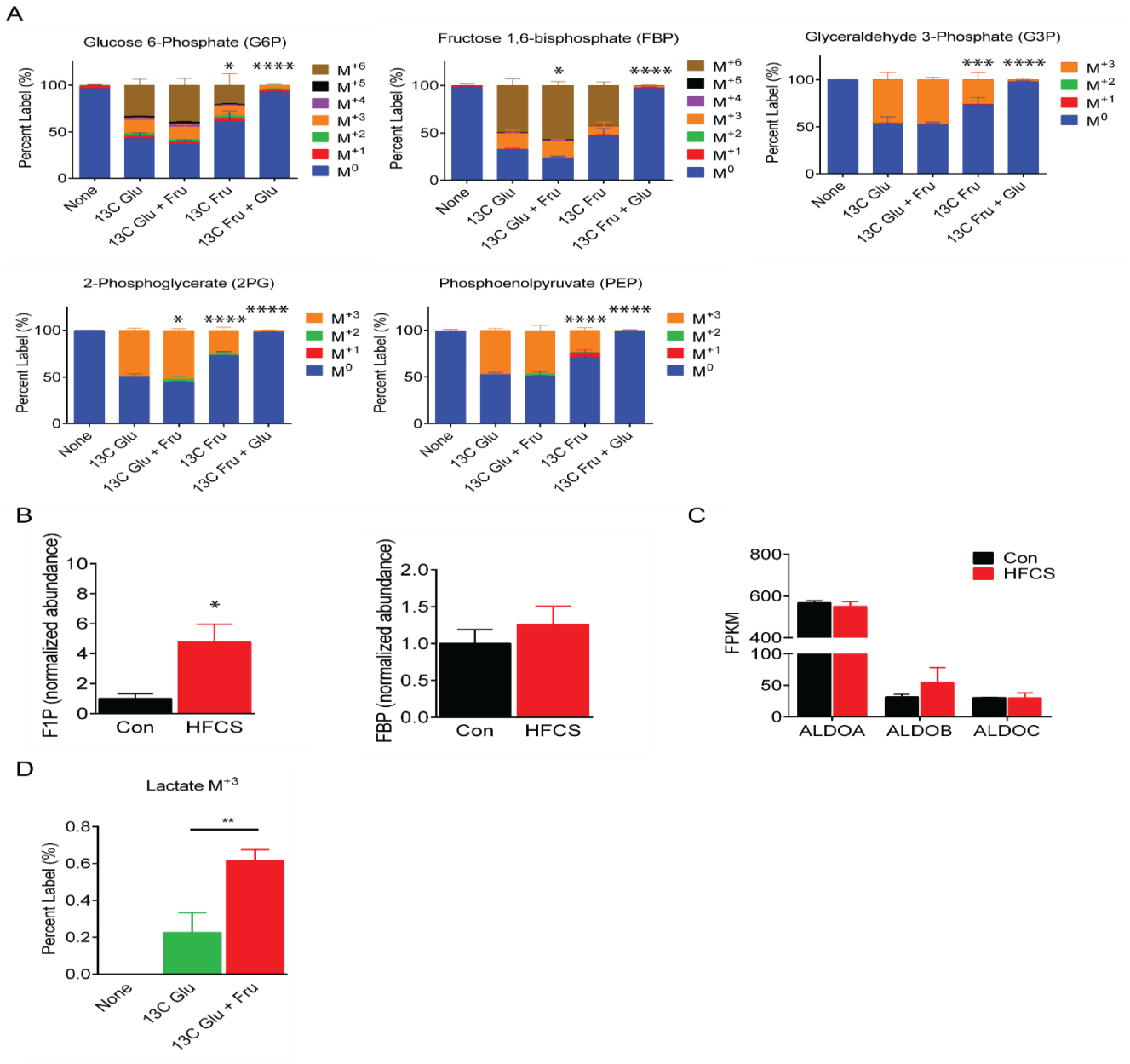

fig. S6. Intestinal tumors facilitate glycolysis by using both glucose and fructose.

(A) Percent labeling of the indicated metabolite following a 10 min *ex vivo* incubation with 10 mM U-[^{13}C]-Glucose (13C Glu), 13C Glu with 10 mM fructose (Fru), 10 mM U-[^{13}C]-Fructose (13C Fru), and 13C Fru with 10 mM Glucose (Glu). n=3 to 4 per group. Two-way ANOVA with Holm-Sidak post-test compared to 13C Glu condition. **P*<0.05, *****P*<0.0001. (B) Relative abundance of fructose 1-phosphate (F1P) and fructose 1,6-bisphosphate (FBP) in APC$^{-/-}$ tumors treated with HFCS *ex vivo* for 10 minutes. Con (n= 3), HFCS (n= 5). Student *t*-test, **P*<0.05, (C) Gene expression of aldolases (ALDOA, Adolase A; ALDOB, Adolase B; ALDOC, Aldolase C) in APC$^{-/-}$ tumors treated with a daily oral gavage of water (Con) or HFCS (HFCS) for 8 weeks. Reported as Fragments Per Kilobase of transcript per Million mapped reads (FPKM). n=4 per group. Comparison was made using t-tests with correction for multiple comparisons using Holm-Sidak method (no significant changes). (D) Percent of fully labeled (M^{+3}) lactate isolated from tumors of APC$^{-/-}$ mice 2 hours following an oral bolus of 400µL containing no sugar (None), 25% 13C-Glu, or 12.5% 13C-Glu + 12.5% Fru. None (n= 4), 13C Glu (n= 7), 13C Glu + Fru (n= 14) tumors taken from n= 2, 4, and 7 mice, respectively. Student's t-test. ***P*<0.01. All data represent means ± S.E.M.

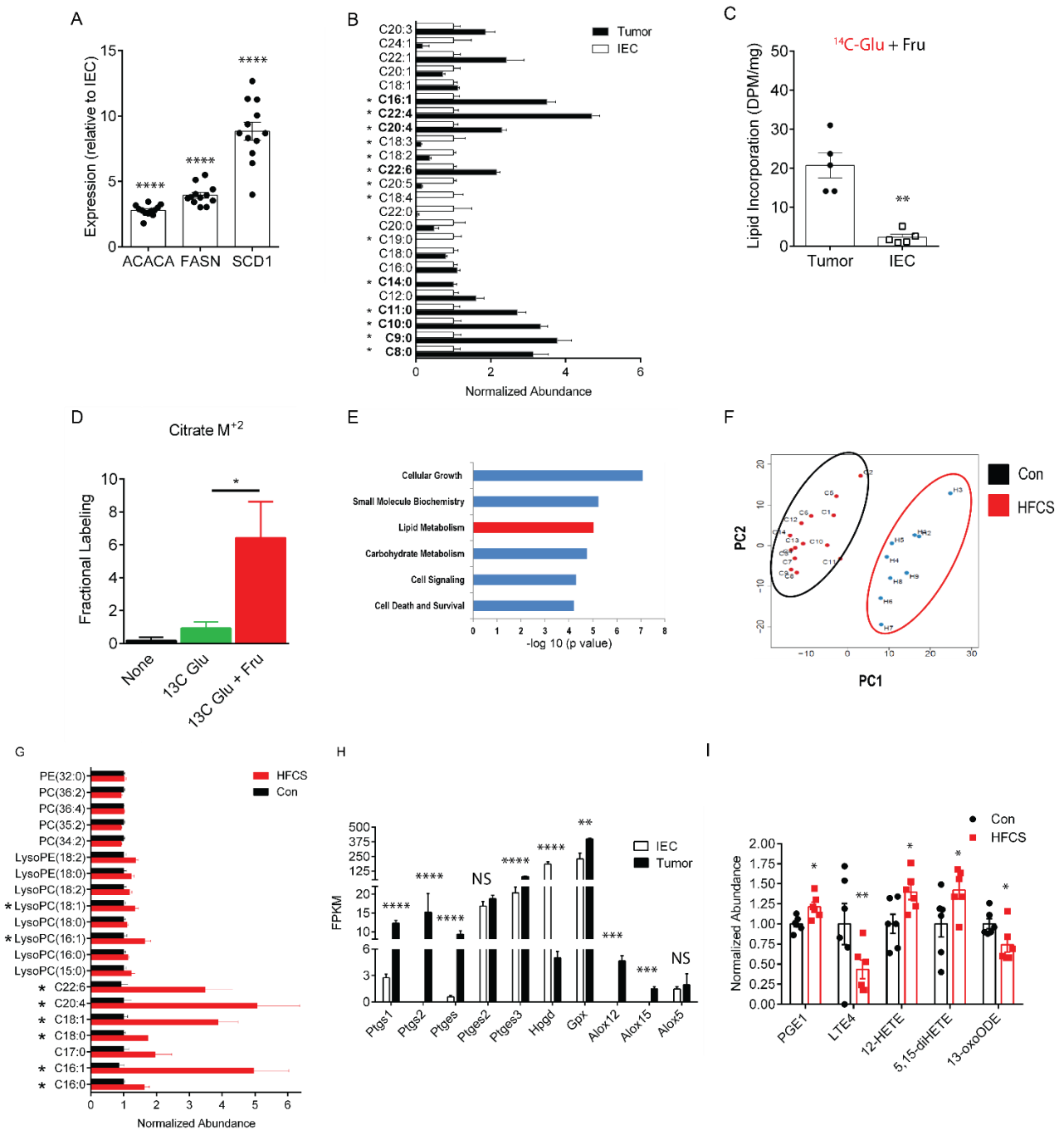

fig. S7. High-fructose corn syrup treatment increases *de novo* fatty acid synthesis in tumor.

(A) Relative expression of key *de novo* lipogenesis genes from APC$^{-/-}$ tumors compared to Intestinal Epithelial Cells (IEC) by quantitative PCR. n=12 per group. Comparisons made by using one-sample *t*-test comparing to a hypothetical value of 1, ****P<0.0001. (B) Normalized abundance of saturated and unsaturated fatty acids from APC$^{-/-}$ tumors compared to IEC. IEC (n= 7), tumor (n=12) Comparison was made using t-tests with correction for multiple comparisons using Holm-Sidak method, Asterisk indicates P<0.01. Bolded fatty acids are increased in tumor vs IEC. (C) The amount of radioactivity in the lipid (non-polar) extract of APC$^{-/-}$ tumors and IECs 4 hours after a bolus of HFCS containing 5 µCi U-[^{14}C]-glucose. Radioactivity amount is presented as disintegrations per minute (DPM) per milligram of protein input. n=5 per group. Tumor and IEC compared by student's *t*-test **P<0.01. Glu, Glucose; Fru, Fructose. (D) Percent of labeled (M^{+2}) citrate following a 10 min *ex vivo* incubation with no sugar (None), 10 mM U-[^{13}C]-Glucose (13C Glu), or 13C Glu with 10 mM fructose (Fru). n=3 per group. One-way

ANOVA with Holm-Sidak post-test. *P<0.05. (E) Pathway enrichment analysis of LC/MS-derived metabolites from $APC^{-/-}$ tumors treated with a daily oral gavage of HFCS as compared to water-treated $APC^{-/-}$ tumors performed using Ingenuity Pathway Analysis (IPA) software. Top six significantly enriched pathways in HFCS tumors are shown. (F) Principle component analysis (PCA) using untargeted LC/MS metabolomics data from $APC^{-/-}$ tumors treated with a daily oral gavage of water (Con) or HFCS over 8 weeks. Con (n=14), HFCS (n=9) (G) Normalized abundance of lipid species from $APC^{-/-}$ tumors treated with a daily oral gavage of water (Con) or high-fructose corn syrup (HFCS). Con (n=14), HFCS (n=9). Comparison was made using t-tests with correction for multiple comparisons using Holm-Sidak method, Asterisk indicates P<0.01. (H) Gene expression of the indicated genes from $APC^{-/-}$ tumors and intestinal epithelial cells (IEC). Data presented as Fragments Per Kilobase of transcript per Million mapped reads (FPKM). n=4 per group. Student's *t*-test with correction for multiple comparisons using Holm-Sidak method. **P<0.01, ***P<0.001, ****P<0.0001. (I) Normalized abundance of eicosanoid species from $APC^{-/-}$ tumors treated with a daily oral gavage of water (Con) or HFCS over 8 weeks. n=6 per group. Comparison was made using Student's t-test. *P<0.05, **P<0.01. All data represent means ± S.E.M.

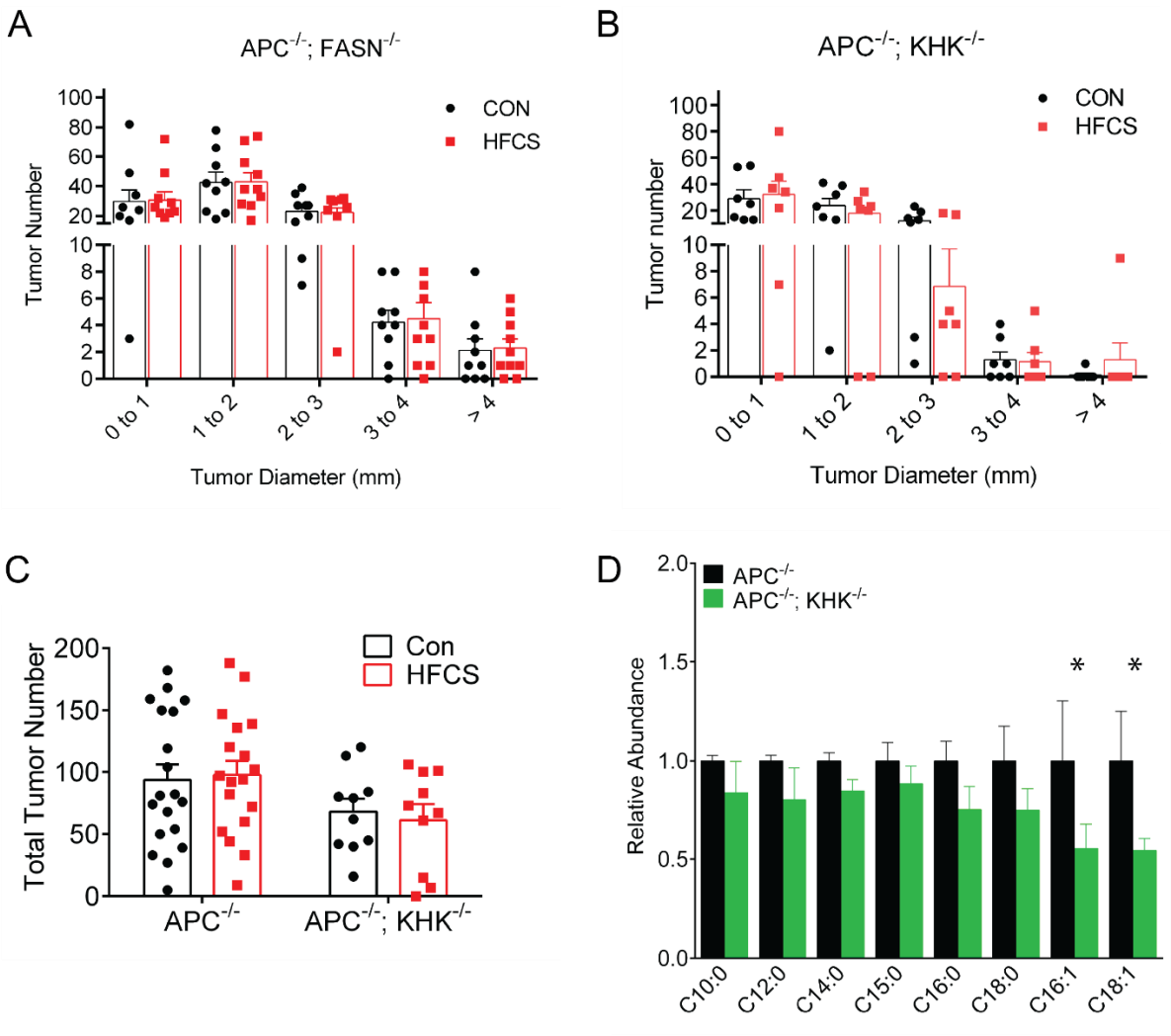

fig. S8. Genetic loss of FASN or KHK abrogates the HFCS-induced shift in tumor size distribution

(A) The size of each tumor (diameter) in the intestine was determined in whole-mount tissue after methylene blue staining, using a dissecting microscope. Shown is the tumor size distribution from APC$^{-/-}$;FASN$^{-/-}$ mice following daily oral gavage of water (Con) or high-fructose corn syrup (HFCS) for 8 weeks. Con (n= 9), HFCS (n=10). Con vs HFCS compared by t-test with correction for multiple comparisons using Holm-Sidak method. No significant differences. (B) Tumor size distribution from Con and HFCS-treated APC$^{-/-}$;KHK$^{-/-}$ mice. n=7 per group. Con vs HFCS compared by t-test with correction for multiple comparisons using Holm-Sidak method. No significant differences. (C) Total number of tumors from APC$^{-/-}$ and APC$^{-/-}$;KHK$^{-/-}$ mice treated with a daily oral gavage of water (Con) or HFCS for 8 weeks. APC$^{-/-}$ Con (n=19) and HFCS (n=18); APC$^{-/-}$; KHK$^{-/-}$ mice, n= 10 per group. Two-way ANOVA showing no significant changes between groups. (D) Relative abundance of saturated and unsaturated fatty acids from APC$^{-/-}$ tumors compared to APC$^{-/-}$; KHK$^{-/-}$ tumors. n=3 per group. Student's *t*-test **P*<0.05. All data represent means ± S.E.M.

References and Notes

1. V. S. Malik, M. B. Schulze, F. B. Hu, Intake of sugar-sweetened beverages and weight gain: A systematic review. *Am. J. Clin. Nutr.* **84**, 274–288 (2006). doi:10.1093/ajcn/84.2.274 Medline

2. A. M. Hodge, J. K. Bassett, R. L. Milne, D. R. English, G. G. Giles, Consumption of sugar-sweetened and artificially sweetened soft drinks and risk of obesity-related cancers. *Public Health Nutr.* **21**, 1618–1626 (2018). doi:10.1017/S1368980017002555 Medline

3. L. Tappy, K. A. Lê, Metabolic effects of fructose and the worldwide increase in obesity. *Physiol. Rev.* **90**, 23–46 (2010). doi:10.1152/physrev.00019.2009 Medline

4. G. M. Singh, R. Micha, S. Khatibzadeh, P. Shi, S. Lim, K. G. Andrews, R. E. Engell, M. Ezzati, D. Mozaffarian; Global Burden of Diseases Nutrition and Chronic Diseases Expert Group (NutriCoDE), Global, Regional, and National Consumption of Sugar-Sweetened Beverages, Fruit Juices, and Milk: A Systematic Assessment of Beverage Intake in 187 Countries. *PLOS ONE* **10**, e0124845 (2015). doi:10.1371/journal.pone.0124845 Medline

5. R. L. Siegel, K. D. Miller, A. Jemal, Colorectal Cancer Mortality Rates in Adults Aged 20 to 54 Years in the United States, 1970-2014. *JAMA* **318**, 572–574 (2017). doi:10.1001/jama.2017.7630 Medline

6. M. Araghi, I. Soerjomataram, M. Jenkins, J. Brierley, E. Morris, F. Bray, M. Arnold, Global trends in colorectal cancer mortality: Projections to the year 2035. *Int. J. Cancer* ijc.32055 (2018). doi:10.1002/ijc.32055 Medline

7. H. Sung, R. L. Siegel, P. S. Rosenberg, A. Jemal, Emerging cancer trends among young adults in the USA: Analysis of a population-based cancer registry. *Lancet Public Health* S2468-2667(18)30267-6 (2019). doi:10.1016/S2468-2667(18)30267-6 Medline

8. M. A. Fuchs, K. Sato, D. Niedzwiecki, X. Ye, L. B. Saltz, R. J. Mayer, R. B. Mowat, R. Whittom, A. Hantel, A. Benson, D. Atienza, M. Messino, H. Kindler, A. Venook, S. Ogino, K. Wu, W. C. Willett, E. L. Giovannucci, J. A. Meyerhardt, Sugar-sweetened beverage intake and cancer recurrence and survival in CALGB 89803 (Alliance). *PLOS ONE* **9**, e99816 (2014). doi:10.1371/journal.pone.0099816 Medline

9. M. Bardou, A. N. Barkun, M. Martel, Obesity and colorectal cancer. *Gut* **62**, 933–947 (2013). doi:10.1136/gutjnl-2013-304701 Medline

10. B. D. Hopkins, M. D. Goncalves, L. C. Cantley, Obesity and Cancer Mechanisms: Cancer Metabolism. *J. Clin. Oncol.* **34**, 4277–4283 (2016). doi:10.1200/JCO.2016.67.9712 Medline

11. J. Yun, E. Mullarky, C. Lu, K. N. Bosch, A. Kavalier, K. Rivera, J. Roper, I. I. C. Chio, E. G. Giannopoulou, C. Rago, A. Muley, J. M. Asara, J. Paik, O. Elemento, Z. Chen, D. J. Pappin, L. E. Dow, N. Papadopoulos, S. S. Gross, L. C. Cantley, Vitamin C selectively kills KRAS and BRAF mutant colorectal cancer cells by targeting GAPDH. *Science* **350**, 1391–1396 (2015). doi:10.1126/science.aaa5004 Medline

12. N. Barker, R. A. Ridgway, J. H. van Es, M. van de Wetering, H. Begthel, M. van den Born, E. Danenberg, A. R. Clarke, O. J. Sansom, H. Clevers, Crypt stem cells as the cells-of-origin of intestinal cancer. *Nature* **457**, 608–611 (2009). doi:10.1038/nature07602 Medline

13. E. R. Fearon, B. Vogelstein, A genetic model for colorectal tumorigenesis. *Cell* **61**, 759–767 (1990). doi:10.1016/0092-8674(90)90186-I Medline

14. V. Fulgoni 3rd, High-fructose corn syrup: Everything you wanted to know, but were afraid to ask. *Am. J. Clin. Nutr.* **88**, 1715S (2008). doi:10.3945/ajcn.2008.25825A Medline

15. Y. Feng, K. Sentani, A. Wiese, E. Sands, M. Green, G. T. Bommer, K. R. Cho, E. R. Fearon, Sox9 induction, ectopic Paneth cells, and mitotic spindle axis defects in mouse colon adenomatous epithelium arising from conditional biallelic Apc inactivation. *Am. J. Pathol.* **183**, 493–503 (2013). doi:10.1016/j.ajpath.2013.04.013 Medline

16. L. A. Drozdowski, A. B. R. Thomson, Intestinal sugar transport. *World J. Gastroenterol.* **12**, 1657–1670 (2006). doi:10.3748/wjg.v12.i11.1657 Medline

17. W. J. Ravich, T. M. Bayless, M. Thomas, Fructose: Incomplete intestinal absorption in humans. *Gastroenterology* **84**, 26–29 (1983). Medline

18. J. J. Rumessen, E. Gudmand-Høyer, Absorption capacity of fructose in healthy adults. Comparison with sucrose and its constituent monosaccharides. *Gut* **27**, 1161–1168 (1986). doi:10.1136/gut.27.10.1161 Medline

19. P. L. Beyer, E. M. Caviar, R. W. McCallum, Fructose intake at current levels in the United States may cause gastrointestinal distress in normal adults. *J. Am. Diet. Assoc.* **105**, 1559–1566 (2005). doi:10.1016/j.jada.2005.07.002 Medline

20. C. Jang, S. Hui, W. Lu, A. J. Cowan, R. J. Morscher, G. Lee, W. Liu, G. J. Tesz, M. J. Birnbaum, J. D. Rabinowitz, The Small Intestine Converts Dietary Fructose into Glucose and Organic Acids. *Cell Metab.* **27**, 351–361.e3 (2018). doi:10.1016/j.cmet.2017.12.016 Medline

21. A. Godoy, V. Ulloa, F. Rodríguez, K. Reinicke, A. J. Yañez, Mde. L. García, R. A. Medina, M. Carrasco, S. Barberis, T. Castro, F. Martínez, X. Koch, J. C. Vera, M. T. Poblete, C. D. Figueroa, B. Peruzzo, F. Pérez, F. Nualart, Differential subcellular distribution of glucose transporters GLUT1-6 and GLUT9 in human cancer: Ultrastructural localization of GLUT1 and GLUT5 in breast tumor tissues. *J. Cell. Physiol.* **207**, 614–627 (2006). doi:10.1002/jcp.20606 Medline

22. Q. Li, Y. Li, J. Xu, S. Wang, Y. Xu, X. Li, S. Cai, Aldolase B Overexpression is Associated with Poor Prognosis and Promotes Tumor Progression by Epithelial-Mesenchymal Transition in Colorectal Adenocarcinoma. *Cell. Physiol. Biochem.* **42**, 397–406 (2017). doi:10.1159/000477484 Medline

23. A. Uzozie, P. Nanni, T. Staiano, J. Grossmann, S. Barkow-Oesterreicher, J. W. Shay, A. Tiwari, F. Buffoli, E. Laczko, G. Marra, Sorbitol dehydrogenase overexpression and other aspects of dysregulated protein expression in human precancerous colorectal neoplasms: A quantitative proteomics study. *Mol. Cell. Proteomics* **13**, 1198–1218 (2014). doi:10.1074/mcp.M113.035105 Medline

24. T. Jensen, M. F. Abdelmalek, S. Sullivan, K. J. Nadeau, M. Green, C. Roncal, T. Nakagawa, M. Kuwabara, Y. Sato, D.-H. Kang, D. R. Tolan, L. G. Sanchez-Lozada, H. R. Rosen, M. A. Lanaspa, A. M. Diehl, R. J. Johnson, Fructose and sugar: A major mediator of non-alcoholic fatty liver disease. *J. Hepatol.* **68**, 1063–1075 (2018). doi:10.1016/j.jhep.2018.01.019 Medline

25. S. A. Hannou, D. E. Haslam, N. M. McKeown, M. A. Herman, Fructose metabolism and metabolic disease. *J. Clin. Invest.* **128**, 545–555 (2018). doi:10.1172/JCI96702 Medline

26. G. Van den Berghe, Fructose: Metabolism and short-term effects on carbohydrate and purine metabolic pathways. *Prog. Biochem. Pharmacol.* **21**, 1–32 (1986). Medline

27. R. C. Morris Jr., K. Nigon, E. B. Reed, Evidence that the severity of depletion of inorganic phosphate determines the severity of the disturbance of adenine nucleotide metabolism in the

liver and renal cortex of the fructose-loaded rat. *J. Clin. Invest.* **61**, 209–220 (1978). doi:10.1172/JCI108920 Medline

28. R. G. Kemp, L. G. Foe, Allosteric regulatory properties of muscle phosphofructokinase. *Mol. Cell. Biochem.* **57**, 147–154 (1983). doi:10.1007/BF00849191 Medline

29. E. Currie, A. Schulze, R. Zechner, T. C. Walther, R. V. Farese Jr., Cellular fatty acid metabolism and cancer. *Cell Metab.* **18**, 153–161 (2013). doi:10.1016/j.cmet.2013.05.017 Medline

30. J. A. Menendez, R. Lupu, Fatty acid synthase and the lipogenic phenotype in cancer pathogenesis. *Nat. Rev. Cancer* **7**, 763–777 (2007). doi:10.1038/nrc2222 Medline

31. I. J. Lodhi, L. Yin, A. P. L. Jensen-Urstad, K. Funai, T. Coleman, J. H. Baird, M. K. El Ramahi, B. Razani, H. Song, F. Fu-Hsu, J. Turk, C. F. Semenkovich, Inhibiting adipose tissue lipogenesis reprograms thermogenesis and PPARγ activation to decrease diet-induced obesity. *Cell Metab.* **16**, 189–201 (2012). doi:10.1016/j.cmet.2012.06.013 Medline

32. T. Ishimoto, M. A. Lanaspa, M. T. Le, G. E. Garcia, C. P. Diggle, P. S. Maclean, M. R. Jackman, A. Asipu, C. A. Roncal-Jimenez, T. Kosugi, C. J. Rivard, S. Maruyama, B. Rodriguez-Iturbe, L. G. Sánchez-Lozada, D. T. Bonthron, Y. Y. Sautin, R. J. Johnson, Opposing effects of fructokinase C and A isoforms on fructose-induced metabolic syndrome in mice. *Proc. Natl. Acad. Sci. U.S.A.* **109**, 4320–4325 (2012). doi:10.1073/pnas.1119908109 Medline

33. C. P. Diggle, M. Shires, D. Leitch, D. Brooke, I. M. Carr, A. F. Markham, B. E. Hayward, A. Asipu, D. T. Bonthron, Ketohexokinase: Expression and localization of the principal fructose-metabolizing enzyme. *J. Histochem. Cytochem.* **57**, 763–774 (2009). doi:10.1369/jhc.2009.953190 Medline

34. R. D. Feinman, E. J. Fine, Fructose in perspective. *Nutr. Metab. (Lond.)* **10**, 45 (2013). doi:10.1186/1743-7075-10-45 Medline

35. G. Livesey, Fructose ingestion: Dose-dependent responses in health research. *J. Nutr.* **139**, 1246S–1252S (2009). doi:10.3945/jn.108.097949 Medline

36. E. H. Yau, I. R. Kummetha, G. Lichinchi, R. Tang, Y. Zhang, T. M. Rana, Genome-Wide CRISPR Screen for Essential Cell Growth Mediators in Mutant KRAS Colorectal Cancers. *Cancer Res.* **77**, 6330–6339 (2017). doi:10.1158/0008-5472.CAN-17-2043 Medline

37. H. Kim, E. L. Giovannucci, Sex differences in the association of obesity and colorectal cancer risk. *Cancer Causes Control* **28**, 1–4 (2017). doi:10.1007/s10552-016-0831-5 Medline

38. P. Mystkowski, E. Shankland, S. A. Schreyer, R. C. LeBoeuf, R. S. Schwartz, D. E. Cummings, M. Kushmerick, M. W. Schwartz, Validation of whole-body magnetic resonance spectroscopy as a tool to assess murine body composition. *Int. J. Obes. Relat. Metab. Disord.* **24**, 719–724 (2000). doi:10.1038/sj.ijo.0801231 Medline

39. M. Yuan, S. B. Breitkopf, X. Yang, J. M. Asara, A positive/negative ion-switching, targeted mass spectrometry-based metabolomics platform for bodily fluids, cells, and fresh and fixed tissue. *Nat. Protoc.* **7**, 872–881 (2012). doi:10.1038/nprot.2012.024 Medline

40. W. Lu, X. Su, M. S. Klein, I. A. Lewis, O. Fiehn, J. D. Rabinowitz, Metabolite Measurement: Pitfalls to Avoid and Practices to Follow. *Annu. Rev. Biochem.* **86**, 277–304 (2017). doi:10.1146/annurev-biochem-061516-044952 Medline

41. J. J. Kamphorst, J. Fan, W. Lu, E. White, J. D. Rabinowitz, Liquid chromatography-high resolution mass spectrometry analysis of fatty acid metabolism. *Anal. Chem.* **83**, 9114–9122 (2011). doi:10.1021/ac202220b Medline

42. L. P. S. de Carvalho, H. Zhao, C. E. Dickinson, N. M. Arango, C. D. Lima, S. M. Fischer, O. Ouerfelli, C. Nathan, K. Y. Rhee, Activity-based metabolomic profiling of enzymatic function: Identification of Rv1248c as a mycobacterial 2-hydroxy-3-oxoadipate synthase. *Chem. Biol.* **17**, 323–332 (2010). doi:10.1016/j.chembiol.2010.03.009 Medline

43. T. R. Sana, K. Waddell, S. M. Fischer, A sample extraction and chromatographic strategy for increasing LC/MS detection coverage of the erythrocyte metabolome. *J. Chromatogr. B Analyt. Technol. Biomed. Life Sci.* **871**, 314–321 (2008). doi:10.1016/j.jchromb.2008.04.030 Medline

44. T. Hartman, K. Rhee, Y. Dai, Metabolomics Analysis of Tuberculosis Drug Activity Using an Agilent 6545 Q-TOF LC/MS (2017), (available at https://www.agilent.com/cs/library/applications/5991-7970EN.pdf).

45. O. Quehenberger, A. M. Armando, A. H. Brown, S. B. Milne, D. S. Myers, A. H. Merrill, S. Bandyopadhyay, K. N. Jones, S. Kelly, R. L. Shaner, C. M. Sullards, E. Wang, R. C. Murphy, R. M. Barkley, T. J. Leiker, C. R. H. Raetz, Z. Guan, G. M. Laird, D. A. Six, D. W. Russell, J. G. McDonald, S. Subramaniam, E. Fahy, E. A. Dennis, Lipidomics reveals a remarkable diversity of lipids in human plasma. *J. Lipid Res.* **51**, 3299–3305 (2010). doi:10.1194/jlr.M009449 Medline

46. A. Dobin, C. A. Davis, F. Schlesinger, J. Drenkow, C. Zaleski, S. Jha, P. Batut, M. Chaisson, T. R. Gingeras, STAR: Ultrafast universal RNA-seq aligner. *Bioinformatics* **29**, 15–21 (2013). doi:10.1093/bioinformatics/bts635 Medline

47. C. Trapnell, B. A. Williams, G. Pertea, A. Mortazavi, G. Kwan, M. J. van Baren, S. L. Salzberg, B. J. Wold, L. Pachter, Transcript assembly and quantification by RNA-Seq reveals unannotated transcripts and isoform switching during cell differentiation. *Nat. Biotechnol.* **28**, 511–515 (2010). doi:10.1038/nbt.1621 Medline

48. S. Anders, P. T. Pyl, W. Huber, HTSeq—A Python framework to work with high-throughput sequencing data. *Bioinformatics* **31**, 166–169 (2015). doi:10.1093/bioinformatics/btu638 Medline

49. J. A. Blake, J. T. Eppig, J. A. Kadin, J. E. Richardson, C. L. Smith, C. J. Bult; the Mouse Genome Database Group, Mouse Genome Database (MGD)-2017: Community knowledge resource for the laboratory mouse. *Nucleic Acids Res.* **45** (D1), D723–D729 (2017). doi:10.1093/nar/gkw1040 Medline

50. M. I. Love, W. Huber, S. Anders, Moderated estimation of fold change and dispersion for RNA-seq data with DESeq2. *Genome Biol.* **15**, 550 (2014). doi:10.1186/s13059-014-0550-8 Medline

51. P. Di Tommaso, M. Chatzou, E. W. Floden, P. P. Barja, E. Palumbo, C. Notredame, Nextflow enables reproducible computational workflows. *Nat. Biotechnol.* **35**, 316–319 (2017). doi:10.1038/nbt.3820 Medline

52. S. zur Nedden, R. Eason, A. S. Doney, B. G. Frenguelli, An ion-pair reversed-phase HPLC method for determination of fresh tissue adenine nucleotides avoiding freeze-thaw degradation of ATP. *Anal. Biochem.* **388**, 108–114 (2009). doi:10.1016/j.ab.2009.02.017 Medline